Design and Development of Reconfigurable Origami Antennas Based on E-textile Embroidery

Thesis

Presented in Partial Fulfillment of the Requirements for the Degree Bachelors of Science in the Department of Electrical and Computer Engineering of The Ohio State University

By

Shreyas R. Chaudhari

Undergraduate Honors Research Program in Electrical and Computer Engineering

The Ohio State University

2018

Thesis Committee

Prof. Asimina Kiourti, Ph.D., Advisor

Prof. Ryan Harne., Ph.D.

Table of Contents

Research Objectives

1. To identify the effect of an accordion folding pattern on a half-wavelength dipole antenna.

2. To develop a class of robust origami antennas based on E-textiles, rather than paper and fragile conductive materials.

3. To compare the performance of an E-textile based accordion dipole antenna compared to that of uniform, copper-based antennas and simulated antennas.

Abstract

Reconfigurable origami-based antennas capable of mechanically altering their physical geometry can adjust their operational characteristics in real-time (resonance frequency, bandwidth, radiation pattern, etc.). Though flexibility and robustness of the realized antenna prototypes are critical, these requirements have not been concurrently achieved to date due to fragile conductive inks and copper tapes employed in fabrication. As an alternative, this research presents a new class of flexible and robust reconfigurable, origami antennas based on E-textile embroidery. Two foldable accordion-dipole antennas, measuring ~160 mm × 10 mm and ~165 mm × 10 mm, are designed, fabricated via embroidery of silver-coated polymer E-threads, and measured using an RF choke and a bazooka balun to achieve balanced operation, respectively. The employed E-threads enable extreme robustness, as attributed to the strong polymer core, as well as high conductivity, as attributed to the surrounding high-conductivity material. The ~160 mm × 10 mm antenna measured with the RF choke is shown to tune its resonance frequency in the span of 627 MHz to 991 MHz while maintaining over 72% of the original 10-dB bandwidth. Similarly, the ~165 mm × 10 mm antenna measured with the bazooka balun is shown to vary its resonance frequency in the 760 MHz to 1015 MHz range while maintaining over 95% of the original 10-dB bandwidth. These proposed tessellated, E-textile antennas can be easily integrated into clothing and mechanical structures, providing a non-invasive way of quantifying deformation for a wide range of applications.

Acknowledgements

The author would like to acknowledge the work and efforts of all the members of Dr. Kiourti's Wearable and Implantable Technologies (WIT) laboratory and Dr. Harne's Laboratory of Sound and Vibration Research, without whom the work would not have been possible. Additionally, special acknowledgement is given to Mr. Saad Alharbi, a close researcher collaborator with the author on the project detailed in this Thesis.

Vita

Mr. Shreyas R. Chaudhari is currently an undergraduate student at The Ohio State University, Columbus OH, studying Electrical and Computer Engineering. He will receive a B.S. degree in Electrical and Computer Engineering in December of 2018. His previous work experience includes an undergraduate research assistantship at the Ohio State Driving Simulation Lab, and software engineering internships at TATA Consultancy Services and JPMorgan Chase & Co. Additionally, since 2017, he has been a research assistant under Dr. Asimina Kiourti in the ElectroScience Laboratory.

Notable Accomplishments

Journal Papers:

S. Alharbi, S. Chaudhari, A. Inshaar, H. Shah, C. Zou, R.L. Harne, and A. Kiourti. "E-textile origami dipole antennas with graded embroidery for adaptive RF performance." *IEEE Antennas and Wireless Propagation Letters*, 2018.

Conference Proceedings:

C. Zou, S. Chaudhari, S. Alharbi, H. Shah, A. Kiourti, and R.L. Harne. "Investigation of reconfigurable antennas by foldable, E-textile tessellations: modeling and experimentation." *The Journal of the Acoustical Society of America*, 143:1955, Aug. 2018.

S. Chaudhari, S. Alharbi, C. Zou, H. Shah, R.L. Harne, and A. Kiourti. "A new class of reconfigurable origami antennas based on E-textile embroidery." in *Proceedings of 2018 IEEE International Symposium on Antennas and Propagation*, 1196, Boston, Massachusetts, Jul. 2018.

H. Shah, A. Inshaar, C. Zou, S. Chaudhari, S. Alharbi, A. Kiourti, and R.L. Harne, "Multiphysics Modeling and Experimental Validation of Reconfigurable, E-Textile Origami Antennas," ASME 2018 International Design Engineering Technical Conference, Quebec City, Canada, Aug. 26–29, 2018.

Presentations:

S. Alharbi, S. Chaudhari, C. Zou, R. Harne, and A. Kiourti, "E-textile Origami Antennas with Graded Embroidery for Reconfigurable Performance," *Consortium on EM and RF (CERF) Annual Meeting*, Columbus, OH, Aug. 7, 2018.

S. Chaudhari and A. Kiourti, "Design and Development of E-textile Origami Antennas," *Denman Undergraduate Research Forum*, Columbus, OH, Apr. 3, 2018.

S. Chaudhari and A. Kiourti, "Design and Development of E-textile Origami Antennas," *OSU Spring Undergraduate Research Forum*, Mar. 28, 2018.

Scholarships:

OSU Undergraduate Honors Scholarship, 2018

List of Tables

List of Figures

Chapter 1. Introduction

Reconfigurable antennas have been extensively explored in recent years for a wide range of applications that include satellite communications, radars, and wearable wireless systems, among others [1]-[7]. As an example, the ever-increasing requirement for a single device to accommodate a multitude of services/applications at different frequencies (e.g., Wi-Fi, Bluetooth, GSM, LTE, GPS) implies the need for antennas that can reconfigure their operating frequency and, hence, their radio frequency (RF) performance [1]. Accordingly, diverse techniques have been reported to enable antenna reconfiguration, including both electrical and mechanical approaches [3].

The adaptation of the ancient art of folding paper, namely origami, has recently been integrated with electromagnetic theory concepts to realize such reconfigurable antennas [8]-[17]. By adjusting the physical configuration of these antennas, the resonance frequency, operational bandwidth, radiation pattern, and other relevant operational characteristics of the antennas may be tuned in real-time.

Unfortunately, origami based foldable antennas reported to date exhibit limited durability as attributed to the fragility of their constituent materials, Table 1.1 [8]-[17]. Specifically, copper tape and conductive inks are conventionally used to realize the conductive portions of state-of-the-art origami antennas as shown in Figure 1.1 [10], [15]-[17]. Given the extensive mechanical stress that is typically associated with origami folding [8], the former material is prone to delamination while the latter is prone to cracking and deterioration in conductivity [18]. In turn, conventional origami antenna substrates have been implemented using paper and shape memory polymers (SMPs). While paper is

low-cost, recyclable, and readily available, it is not robust to extensive folding. In addition, paper is influenced by environmental factors (humidity, etc.), which, in turn, alter its dielectric properties (permittivity, loss tangent) and life expectancy. SMPs, i.e., polymers that convert into pre-programmed structures under certain stimuli [19], are more robust than paper, but have limited means to adhere to conductors.

Table 1.1: Summary of origami antennas reported in the literature vs. the proposed approach.

Ref.	Antenna Type	Operating Frequency (GHz)	Substrate Material	Conductive Material
[8]	Helical	0.86 – 2.14	Paper	Copper foil
[9]	Helical	4 – 4.5	Plastic	Copper wire
[10]	Monopole array	2 – 4	Paper	Copper tape
[11]	Helical	2.07 – 4.45	Paper	Copper tape
[12]	Microstrip patch	2.0 – 2.3	SMPs	Copper foil
[13]	Yagi-Uda loop array	1.31	Paper	Copper tape
[14]	Patch array	2.3	SMPs	Conductive ink
[15]	Microstrip-fed monopole	0.95 – 1.57	Paper	Copper film
[16]	Dipole	2.1 – 3.5	Paper	Copper tape
[17]	Coplanar waveguide fed, dual band	2.3 - 2.8, 4.1 – 7.0	Paper	Conductive ink
Proposed	Dipole	0.76 – 1.015	Fabric	E-threads

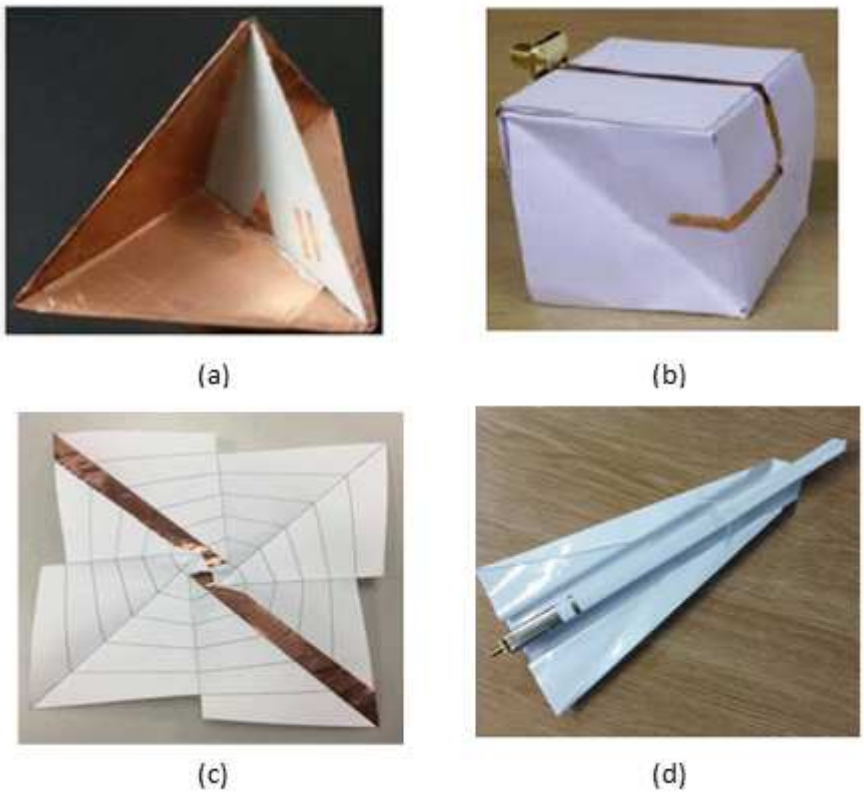

Figure 1.1: Origami antennas reported to date typically utilize copper tape and conductive inks to realize the conductive portions of the antenna: (a) monopole array antenna [10], (b) microstrip fed monopole antenna [15], (c) dipole antenna [16], (d) coplanar waveguide fed, dual-band antenna [17].

As an alternative, this research proposes a new class of origami-based antennas that exhibit reconfigurable performance while also being mechanically robust and durable [19]-[20]. The proposed fabrication approach lies on automated embroidery of silver-coated polymer E-threads [21] to realize conductive surfaces that conform to the shape of the desired origami tessellation [22]-[24]. In this investigation, two accordion-based dipole origami antennas are explored: the first with dimensions ~160 mm × ~10 mm and measured using an RF choke to achieve balanced operation, and the second with dimensions ~165 mm × ~10 mm and measured with a bazooka balun to achieve balanced operation. Simulations and measurements are contrasted for the accordion dipoles to exemplify the

adaptive antennas. Furthermore, the contrasts between the E-thread and solid copper-based antennas illustrate the efficacy of the concept in comparison to conventional antenna material selection. Excellent agreement exists for all aforementioned prototypes, highlighting the feasibility and potential of our approach. Eventually, the proposed E-textile origami antennas are anticipated to impact applications spanning the life sciences, medical sciences, engineering, and more.

The remainder of the Thesis is organized as follows. Chapter 2 provides a brief background on the operation principles of traditional dipole antennas. The simulation setup, fabrication process, and experimental setup for the accordion dipole antennas are described in Chapter 3. Chapter 4 contains the simulated and experimental results for the proposed antennas. Future research recommendations and possible applications are described in Chapter 5, followed by the conclusion of the Thesis in Chapter 6.

Chapter 2. Dipole Antennas: Theory and Accordion-Based Reconfigurability

2.1. Operating Principle of Dipole Antennas

The half-wavelength dipole antenna is selected as the basis of the proposed accordion antenna, due to its popularity in the field as well as its simple fabrication process [25]. Dipole antennas consist of two conducting segments that are separated at the center, with an alternating current (AC) power supply connected at the separation point (namely, feed point). Due to the periodic change in direction of the current within the conducting segments, as determined by the frequency setting of the power source, standing current waves are generated along the length of the antenna [26]. This standing wave causes the ends of the antenna to become oppositely charged, hence the characterizing term "dipole" in the antenna name, Figure 2.1 [27].

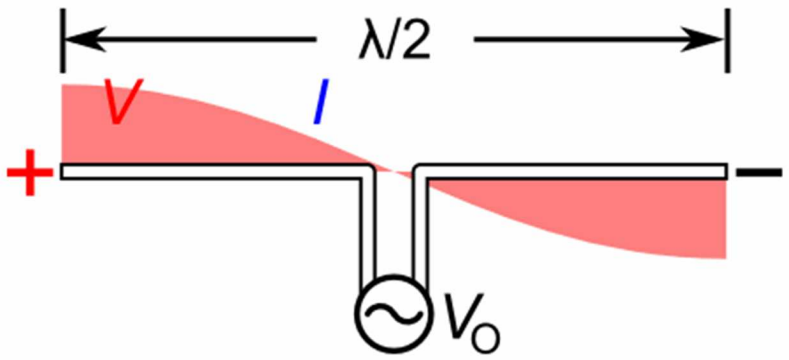

Figure 2.1: Standing current wave along length of the half-wavelength dipole antenna causes ends to become oppositely charged. V_o is the AC power source. The wavelength of the antenna is denoted by λ [27].

The half-wavelength dipole antenna radiates due to the alternating current within its structure. Each charged particle in space produces a surrounding electric field. The electric field is defined as the vector force quantity that would act upon a single positive charge at each point in space [28]. For example, Figure 2.2 shows the electric field lines corresponding to a negative charge [29]. As a charge moves, the corresponding electric field is disturbed. The electric field may react to realign with accelerated charge at the speed of light [28]. Hence, in the region immediately surrounding the moving charge, the electric field may realign itself relatively quickly. However, in regions far away from the charge, the field requires more time to realign [28].

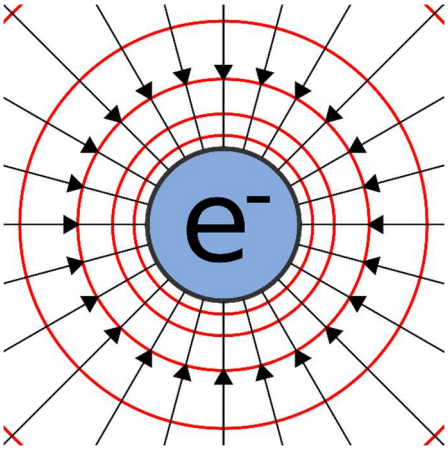

Figure 2.2: Electric field corresponding to an electron (e^-). Proximity of field lines, shown in black, signifies relative strength of the field. Equipotential lines are shown in red [29].

Electromagnetic radiation can thus be observed as the realignment of the electric, and corresponding magnetic, fields due to the acceleration of a charge. As mentioned previously, the current within the conductive segments of the antenna changes direction due to the AC power supply connected at the center of the antenna. In a single AC cycle, charges are accelerated in a specific direction within the antenna. In the following cycle,

charges are accelerated in the opposing direction. The disturbances generated by these accelerations result in propagating electric fields that surround the antenna. The resulting electric fields observed far away from the half-wavelength dipole antenna are demonstrated in Figure 2.3 [27].

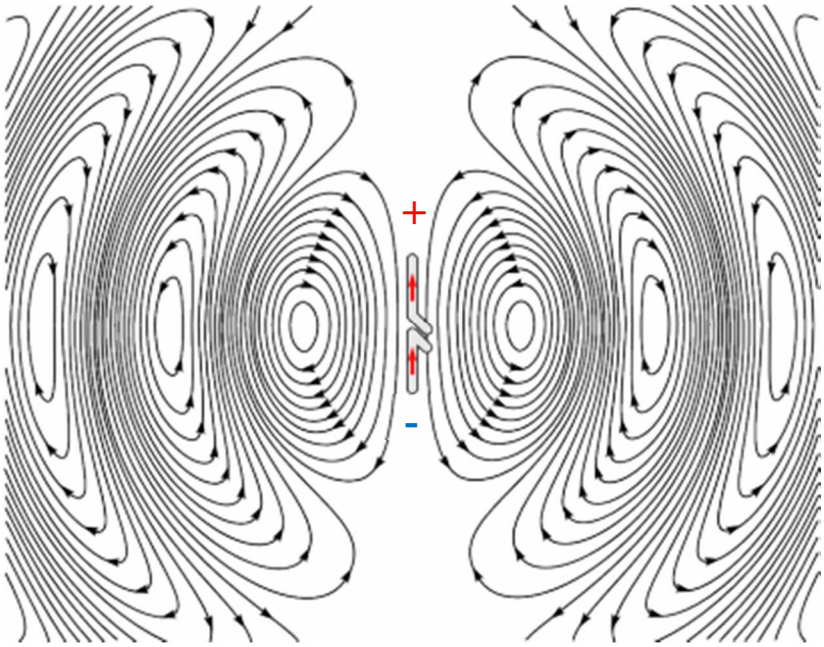

Figure 2.3: Electric fields observed far away from the half-wavelength dipole antenna, resulting from the standing current wave within the antenna [27].

2.2. Parameters of Interest for Dipole Antennas

Resonance Frequency: The half-wavelength dipole exhibits a wavelength that is approximately twice the end-to-end length of the antenna (L) [28]. The operating frequency (f), also known as the resonance frequency, of the half-wavelength dipole as a function of the end-to-end antenna length is given in Equation 1 [28], where (c) is the speed of light

given in meters/second. Thus, as the end-to-end length of the antenna decreases, the operating frequency of the antenna increases.

$$f \approx \frac{c}{2L} \quad (1)$$

The operating frequency of an antenna can be indirectly measured via measurements of its reflection coefficient as a function of frequency, $|S_{11}|$. The $|S_{11}|$ describes the amount of power reflected by the antenna relative to the input power to the antenna, and can be measured using a network analyzer [28]. For example, an $|S_{11}|$ of 0 dB signifies that no power has been radiated by the antenna, as all of the power is reflected back to the source [28]. The frequency at which the minimum magnitude of the S_{11} is observed is therefore defined as the resonance frequency of the antenna. At the resonance frequency, the power transmitted to the antenna results in maximum radiation [28]. An example $|S_{11}|$ plot is shown in Figure 2.4. In this case, the resonance frequency of the half-wavelength dipole antenna is 820 MHz.

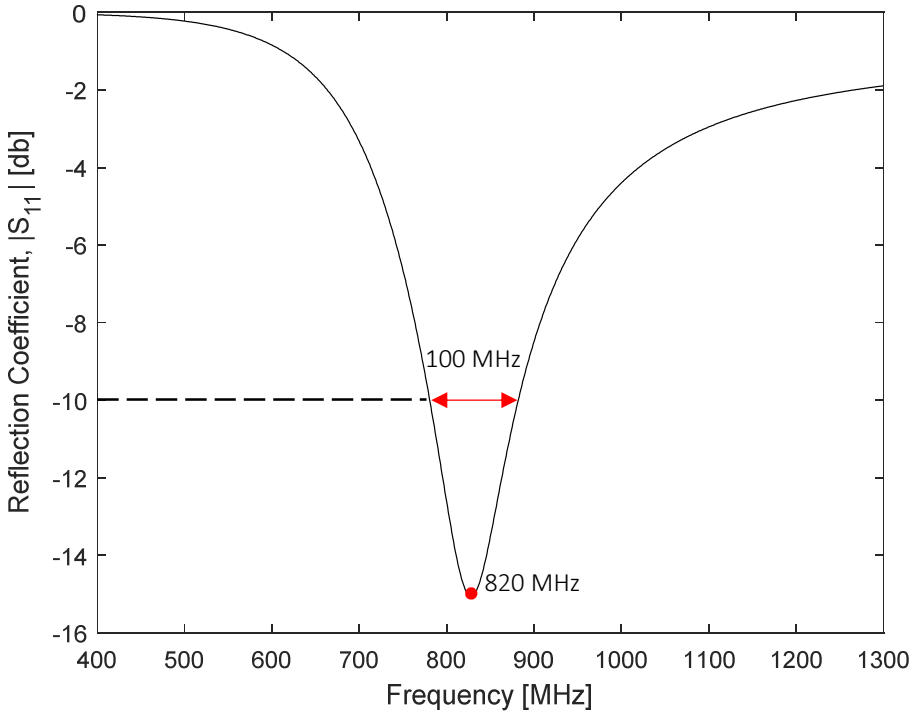

Figure 2.4: Example $|S_{11}|$ plot indicating a resonance frequency of 820 MHz, and a 10-dB bandwidth of 100 MHz.

Bandwidth: The bandwidth of an antenna can be determined from its $|S_{11}|$ plot. The antenna bandwidth defines the range of frequencies over which the antenna can radiate or receive power [28]. In practice, the bandwidth is typically defined at the 10-dB level, however in certain cases the 3-dB (or other level) bandwidth may be reported. As an example, the 10-dB bandwidth of the half-wavelength dipole antenna described in Figure 2.4 is 100 MHz.

Radiation Pattern: The radiation pattern of an antenna displays the power radiated as a function of direction. The radiation pattern is observed in the antenna's far field [28]. The far field is defined by Equation 2 [28], where (L) is the end-to-end length of the antenna, (λ) is the wavelength of the antenna, and (R) is the distance from the antenna.

$$R > \frac{2L^2}{\lambda} \qquad where\ R \gg D, R \gg \lambda \quad (2)$$

Half-wavelength dipole antennas exhibit omnidirectional radiation in the plane perpendicular to antenna axis [25]. The three-dimensional, toroidal radiation pattern of a half-wavelength dipole antenna is illustrated in Figure 2.5. The dipole antenna does not radiate along the ends of the antenna axis.

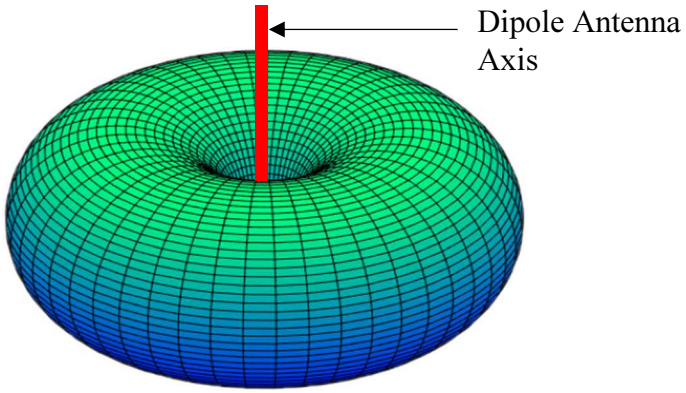

Figure 2.5: 3D radiation pattern of dipole antenna.

The two-dimensional radiation patterns in the plane that contains the electric field (E-plane) and the plane that contains the magnetic field (H-plane) are shown in Figure 2.6 [27].

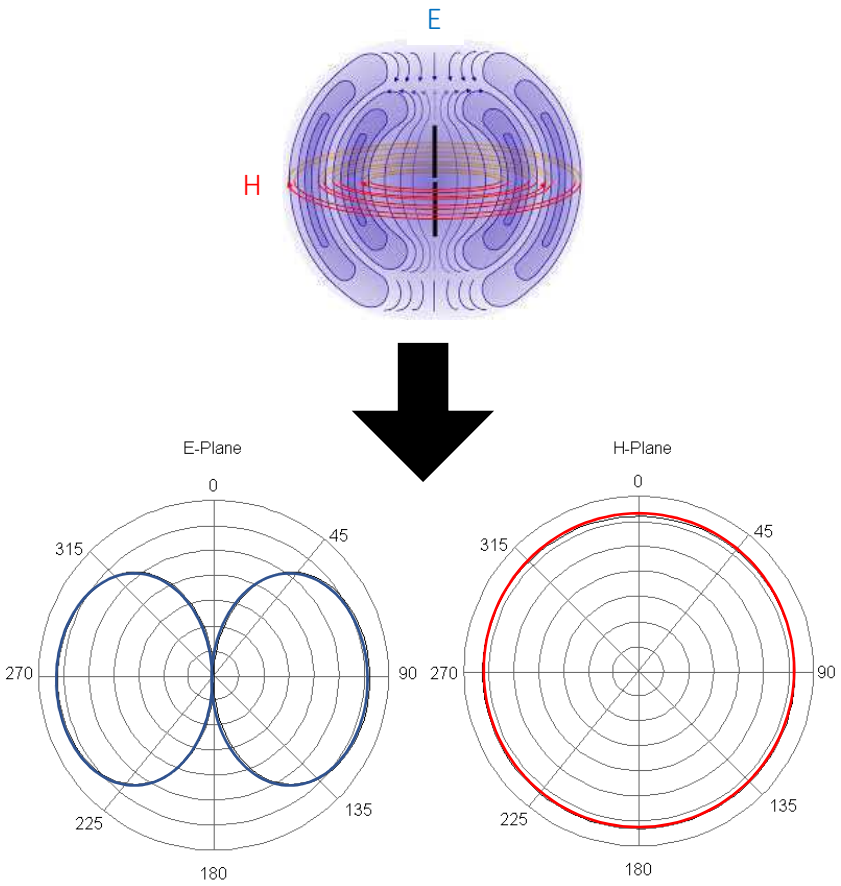

Figure 2.6: Radiation patterns of a half-wavelength dipole antenna in the E-plane and H-plane [27].

Directivity: The directivity (D) of an antenna can be observed from its radiation pattern. The directivity parameter of an antenna describes the relative direction in which a majority of power is radiated or received by an antenna [28]. An antenna that radiates power equally in all directions therefore by definition has a directivity of zero [28]. The directivity of an antenna can be calculated using Equation 3. Equation 3 effectively determines the ratio of the maximum value of radiated power to the average radiated power, using the antenna's normalized radiation pattern in terms of spherical coordinates, $F(\theta, \phi)$ [28].

$$D = \frac{1}{\frac{1}{4\pi}\int_0^{2\pi}\int_0^{\pi}|F(\theta,\phi)|\sin(\theta)\,d\theta d\phi} \quad (3)$$

The directivity of a half-wavelength dipole antenna is typically 2.15 dB, which in practice, is often the lowest directivity that can be achieved without sacrificing antenna efficiency [28].

Efficiency: The efficiency (ε_R) of an antenna describes the amount of power radiated ($P_{radiated}$) by the antenna relative to the amount of power delivered ($P_{delivered}$) to the antenna, as described in Equation 4 [28].

$$\varepsilon_R = \frac{P_{radiated}}{P_{delivered}} \quad (4)$$

Antennas may exhibit reduced efficiency due to losses in the conductive material of the antenna, losses in dielectric materials surrounding the antenna that attenuate the electric fields, and impedance mismatch losses between the transmission line feeding the antenna and the antenna itself [28]. Half-wavelength dipole antennas typically exhibit efficiencies near 100%, assuming no surrounding lossy materials during antenna operation [28].

Antenna Impedance: Antenna impedance (Z) characterizes the voltage and current distributions at the antenna input. The real portion of the impedance represents the amount of power radiated or absorbed by the antenna [28]. The imaginary portion signifies the amount of power stored in the near field region of the antenna [28]. The impedance for a half-wavelength dipole antenna is given in Equation 5 [28].

$$Z = 73 + 42.5j \quad (5)$$

Expectedly, the impedance of the antenna must be matched with that of the transmission line in order to ensure optimal power transfer [28].

Gain: The gain (*G*) parameter of an antenna makes use of both the antenna directivity and efficiency values. Antenna gain effectively measures the antenna's ability to transmit radio waves in a particular direction using the supplied amount of power, as given in Equation 6 [28].

$$G = \varepsilon_R D \quad (6)$$

Therefore, gain is more often used in practice to characterize an antenna's performance compared to directivity, as it accounts for the losses of the antenna. Assuming no electrical losses within the antenna or to surrounding materials, the gain for a half-wavelength dipole antenna is equal to its directivity, that is 2.15 dB [28].

2.3. Ways of Balancing Dipole Antennas

To ensure proper operation of the dipole antenna, current in both conducting segments must be of equal magnitude. When a coaxial cable is used to supply power to a dipole antenna, current is forced to flow from the inner conductor of the coaxial cable to

the corresponding dipole antenna arm. However, current from the interior of the coaxial braid may travel in the reverse direction along the exterior of the braid, as shown in Figure 2.7 [27].

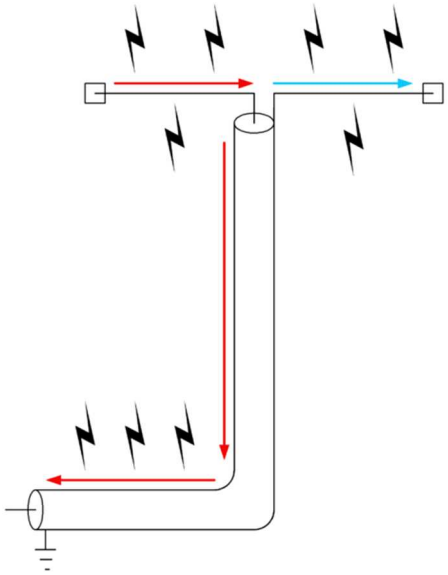

Figure 2.7: Current from interior braid of coaxial cable traveling in reverse direction along exterior of braid, causing the coaxial cable itself to radiate [27].

When current travels along the outer braid of the coaxial cable, then the cable itself acts as a radiating antenna thereby interfering in the measurements of the antenna under test. Radio-frequency (RF) chokes act as inductors, and can therefore be used to eliminate current traveling along the outer braid of the coaxial cable. RF chokes are typically suited for broadband applications. Baluns can also be used to transform the unbalanced power signal from the coaxial cable to a balanced signal that can be supplied to the antenna. A bazooka balun, also known as a sleeve balun, in particular behaves as a short-circuited transmission line. The sleeve is electrically connected to the coaxial cable, causing the current along the interior of the sleeve to be equal in magnitude and opposite in direction to the current flowing along the exterior of the coaxial cable. Thus, the current existing

along the exterior of the coaxial braid is reflected back toward the antenna. A bazooka balun that measures approximately a quarter of the antenna's operating wavelength effectively increases the impedance along the outer coaxial braid to infinity [28]. Consequentially, the current flowing from the inner conductor to a given dipole arm is equal to the current flowing from the outer conductor resulting in balanced operation of the antenna. Baluns are typically specified to operate within a narrow band, as compared to RF chokes. Copper tape antennas equipped with a bazooka balun and RF choke are pictured in Figure 2.8 (a) and Figure 2.8 (b) respectively.

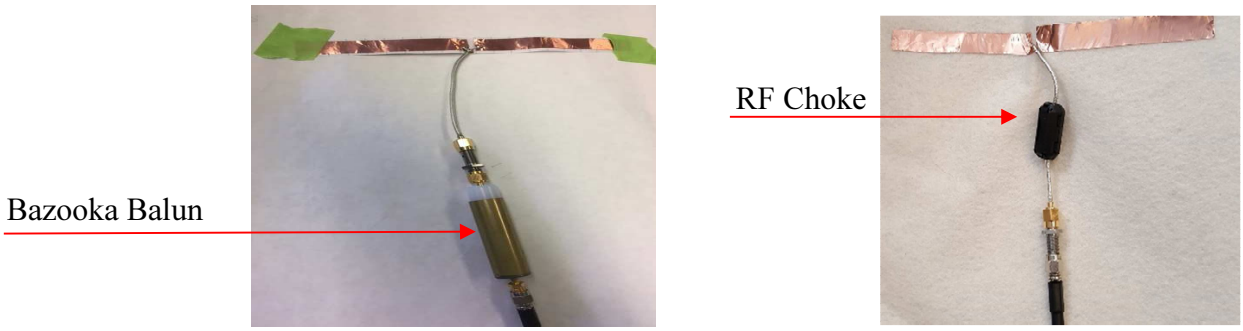

(a) (b)

Figure 2.8: Copper tape antennas equipped with (a) bazooka balun and (b) RF choke.

2.4 Operating Principle of Accordion-Based Origami Dipole

The operation of an origami, accordion-based, half-wavelength dipole antenna is demonstrated in Figure 2.9. The given antenna is theoretically capable of tuning its resonance frequency over a range of 300 MHz. Expectedly, as the antenna folds, the length of the current flow upon the antenna decreases, and the antenna resonant frequency increases accordingly. Similarly, as the antenna unfolds, the length of the current flow upon the antenna increases, resulting in a decreased resonant frequency. For the example case

shown in Figure 2.9, a traditional dipole antenna measuring ~200 mm exhibits an operating frequency of 700 MHz. Likewise, a traditional dipole antenna with a length of ~140 mm operates at 1000 MHz. Therefore, an antenna capable of configuring its end-to-end length in the span of ~200 mm to ~140 mm is capable of tuning its resonance frequency in the 700 MHz to 1000 MHz range respectively.

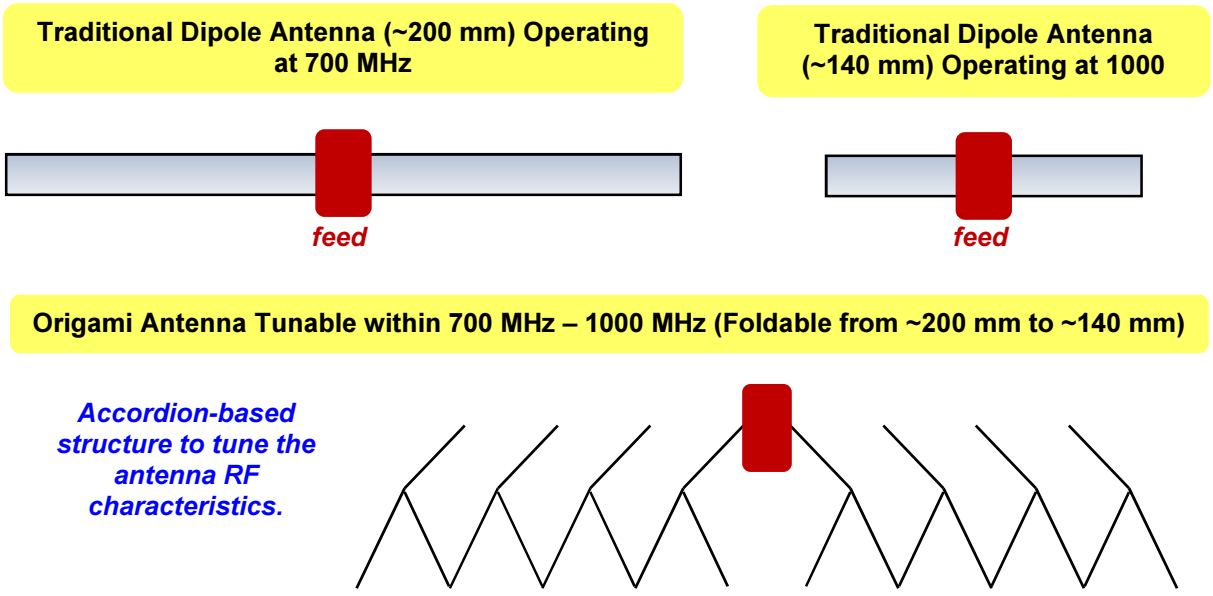

Figure 2.9: Operating principle of an accordion based origami antenna, whose resonance frequency may be manually tuned in the 700 – 1000 MHz range by decreasing the end-to-end length of the antenna by roughly 60 mm.

Chapter 3. Simulation and Experimental Setups

3.1. Simulation Setup

Both dipole antennas explored in this thesis (~160 mm and ~ 165 mm long) are simulated in ANSYS High Frequency Structure Simulator (HFSS™) in order to validate measurement results [30]. Finite Element Method (FEM) simulations are conducted for an equivalently shaped copper, half-wavelength dipole antenna.

The FEM is a mathematical procedure used by HFSS™ to solve electromagnetic problems [31]. As a first step, a three-dimensional model of the antenna is created in HFSS™. The field distributions of the collective antenna model rely on an infinite number of independent variables, and hence cannot be solved mathematically [32]. Hence, the model is subsequently discretized into an interconnected mesh of tetrahedral subsections [31]. The FEM models the electric and magnetic field behavior for each of these tetrahedral subsections using a set of algebraic equations, with a finite number of degrees of freedom. For this reason, each tetrahedral subsection of the antenna mesh is known as a finite element [32]. The electric and magnetic fields within each finite element are subsequently computed. The overall field configuration and corresponding S-parameters for the original antenna model are then determined by merging the boundaries of the finite element results in accordance with Maxwell's equations [31].

As shown in Figure 3.1, the ~160 mm and the ~165 mm copper antennas are simulated with a single fold on each dipole arm. Gain and radiation pattern simulations are conducted only for the ~165 mm antenna, while $|S_{11}|$ reflection coefficient simulations are performed for antennas of both dimensions. Simulations are performed over a frequency sweep of 0.2 to 1.5 GHz. In HFSS™, the electric and magnetic fields in the far-field are

computed with the help of a user-defined radiation boundary [31]. In the simulation of the ~160 mm and ~165 mm copper antennas, an air box is selected as the radiation boundary. The dimensions of the air box are defined such that the distance from the antenna to the air box boundary is greater than a quarter of the antenna's operational wavelength. Specifically, the air box is configured such that the distance from the antenna to the air box is about 10 cm at the flat and 20° positions, 9 cm at the 40° position, and 8 cm at the 60° position for both the ~160 mm and ~165 mm antennas.

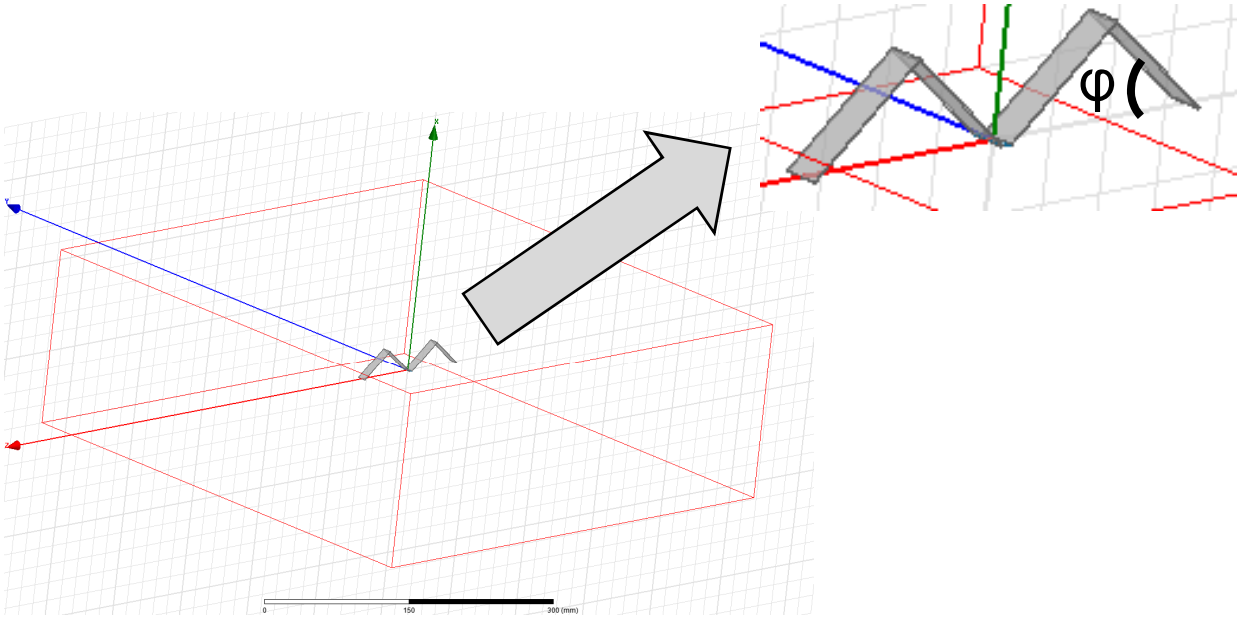

Figure 3.1: HFSS simulation setup, including the airbox, for a copper dipole antenna. Fold angle φ is defined as the angle between the copper antenna arm and the XY plane.

3.2. Antenna Fabrication

A diagram of the proposed embroidery process used to realize E-textile origami antennas is shown in Figure 3.2. As a first step, the origami antenna is designed by computer modeling to understand ideal performance characteristics (e.g., Ansys HFSS [30] or COMSOL Multiphysics® [33]). Next, a Windows Metafile (WMF) of the aforementioned design is created, and further imported into Brother's Personal Embroidery Design Software System (PE-DESIGN) for digitization [34]. Digitization implies identification of the path that the needle will follow during embroidery, stitch by stitch. That is, at this point, the embroidery density can be manually adjusted. For high surface conductivity, comparable to that of copper, the E-textile antennas are fabricated with a uniform density of 7 E-threads/mm. The aforementioned density is the maximum supported by the embroidery machine. The selected Elektrisola® EE-threads exhibit a low DC resistance of 1.9 Ω/m, and a diameter of only 0.12 mm that enabled embroidery precision as high as ~0.1 mm [35].

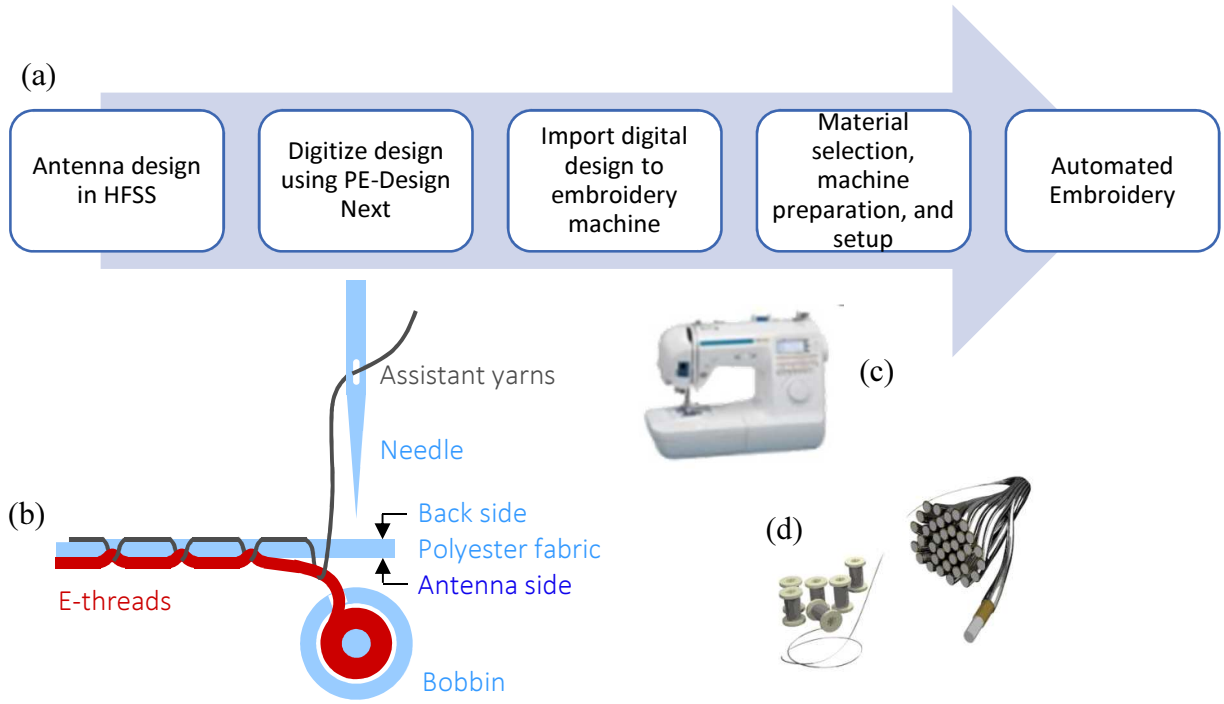

Figure 3.2: Diagram of the complete E-textile fabrication procedure, including the step-by-step embroidery process (a), sewing mechanism (b), Brother embroidery machine (c), and employed 0.12 mm diameter E-threads (d).

Two half-wavelength, E-textile dipole antenna prototypes are fabricated with overall lengths of ~160 mm and ~165 mm. Both E-textile antennas exhibit widths of ~10 mm. These prototypes are embroidered upon organza fabric that exhibits dielectric properties (permittivity, loss tangent) similar to air. For comparison, two half-wavelength antennas are also fabricated using copper-tape to realize the antenna surface. The copper-tape antennas exhibit dimensions equivalent to those of the corresponding E-textile antennas. The copper segments are adhered to the organza fabric by means of an adhesive-backed copper tape. An E-textile antenna with its corresponding copper antenna is shown in Figure 3.3.

(a) (b)

Figure 3.3: Fabricated antennas (a) E-textile, (b) Copper.

The antennas were fabricated at lengths of ~160 mm and ~165 mm to ensure that the resonance frequencies of the antennas remained within the ultra-high frequency range. The ultra-high frequency range includes frequencies from 300 to 3,000 MHz, which correspond to wavelengths of 1 m and 0.1 m respectively. If the antennas were fabricated to operate at much higher frequencies, the simulation would have to be modified in order to more accurately model the E-textile antennas. Significantly higher frequencies correspond to very small wavelengths. Small thread gaps present in the E-textile antennas could therefore result in reduced conductivity. Hence, in order to accurately model the reduced conductivity of the E-textile antennas at such frequencies, the simulation would need to be adjusted either by choosing a material of lower conductivity, or implementing similar gaps in the antenna model. By designing the antenna to operate within the very high frequency range, these modifications could be avoided.

3.3. Experimental Setup

The effect of a single fold upon each arm of the dipole antenna is explored in this investigation per Figure 3.1. In order to accurately study the antennas at several accordion fold positions, two groups of four Styrofoam fixtures are fabricated for a total of eight

fixtures. The Styrofoam fixtures exhibit a saw-tooth like pattern, as pictured in Figure 3.4. The first group of Styrofoam fixtures are specifically dimensioned to accommodate the ~160 mm antennas, while the second group of fixtures are designed to accommodate the ~165 mm antennas. Within each group, each Styrofoam fixture exhibit a different angle measured from the base of the fixture to the diagonal edge, shown as φ in Figure 3.4. The fixtures are created for angles of 20°, 40°, and 60°. With the assistance of the Laboratory of Sound and Vibration Research (LSVR), a laser cutter was used to form the Styrofoam fixtures in order to ensure dimensional precision.

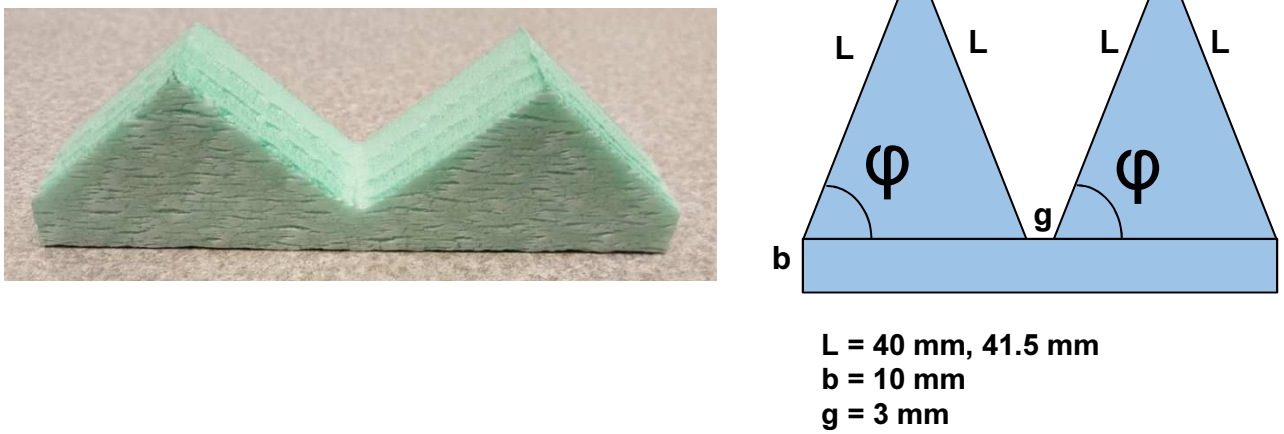

Figure 3.4: Styrofoam fixture used in the experiment, with φ = 20°, 40°, and 60°. L = 40 mm was used to fabricate fixtures that could accommodate ~160 mm antennas, while L = 41.5 mm was used for ~165 mm antenna fixtures. Fabrication was accomplished with the support of the LSVR.

The antennas are securely fastened upon the fixtures using either lossless toothpicks or tape, both of which exhibit permittivity values close to air. Antenna measurements are

recorded for each textile and copper antenna when the antenna is flat and when the antenna is fastened in each of the three dimensionally appropriate Styrofoam fixtures. Reflection coefficient and realized gain measurements are recorded via a network analyzer and EMScan's RFxpert [27], respectively. In particular, EMScan's RFxpert consists of a physical test bed and software package that measures the near field radiation in order to extrapolate the far field characteristics.

A coaxial cable is used to feed the ~160 mm antenna and a ferrite-core RF choke is employed to eliminate current along the outer braid of the coaxial cable. For the ~165 mm antenna, bazooka baluns tuned at the antennas' resonance frequencies are used to connect the balanced dipole antenna to the unbalanced coaxial cable. Specifically, three different bazooka baluns are employed to cover the full ~700 to ~1100 MHz operating frequency range of the origami-based antenna. The experimental setups for both antenna dimensions are shown in Figure 3.5.

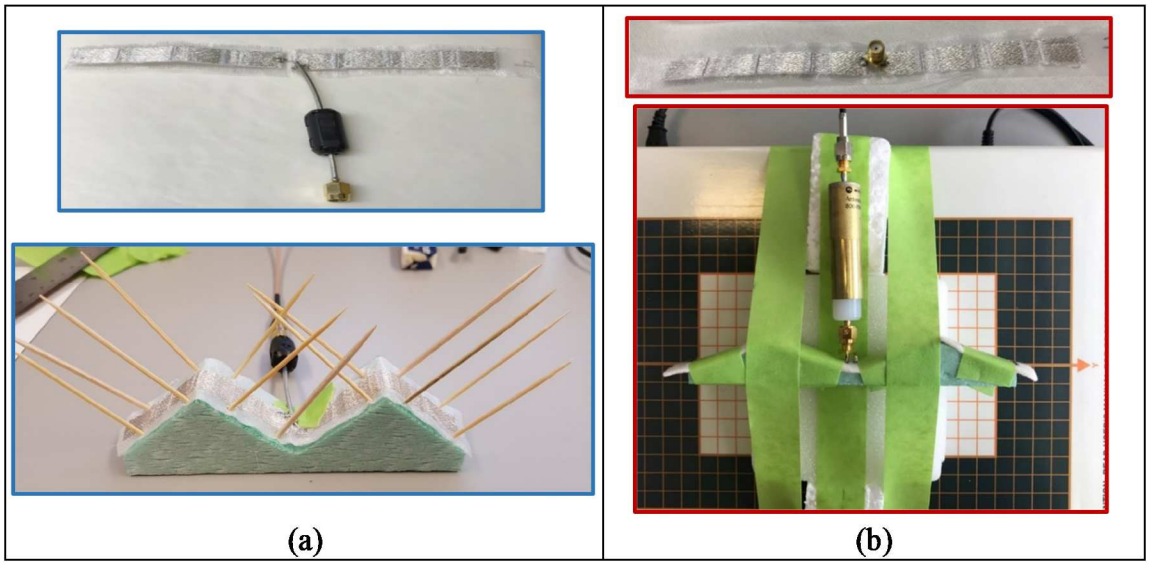

Figure 3.5: Experimental setup of (a) ~160 mm antenna measured using RF choke, (b) ~165 mm antenna measuring using bazooka balun, measured on RFxpert test bed

Chapter 4. Results

4.1. Simulation Results

The resonant frequencies for the simulated ~160 mm and ~165 mm uniform copper antennas are shown in Table 4.1. The first column in Table 4.1 gives the angle of inclination at which the corresponding antenna is simulated. Expectedly, an increase in the fold angle of the dipole antenna corresponds to an increase in the antenna's resonance frequency. Furthermore, as defined by Equation 1 in Section 2.2, the resonance frequency of the ~160 mm antenna is on average greater than that of the ~165 mm antenna.

Table 4.1: Simulated resonant frequencies.

Position	Antenna Length: ~ 160 mm	Antenna Length: ~ 165 mm
0˚	0.797 GHz	0.756 GHz
20˚	0.810 GHz	0.792 GHz
40˚	0.860 GHz	0.860 GHz
60˚	0.990 GHz	1.012 GHz

As the fold angle of the antenna increases in simulation, the effective length of the antenna decreases. This feature is made apparent in Figure 4.1, which depicts the simulated surface current distributions of an accordion dipole antenna. As shown, larger fold angles result in a shorter overall path of current flow.

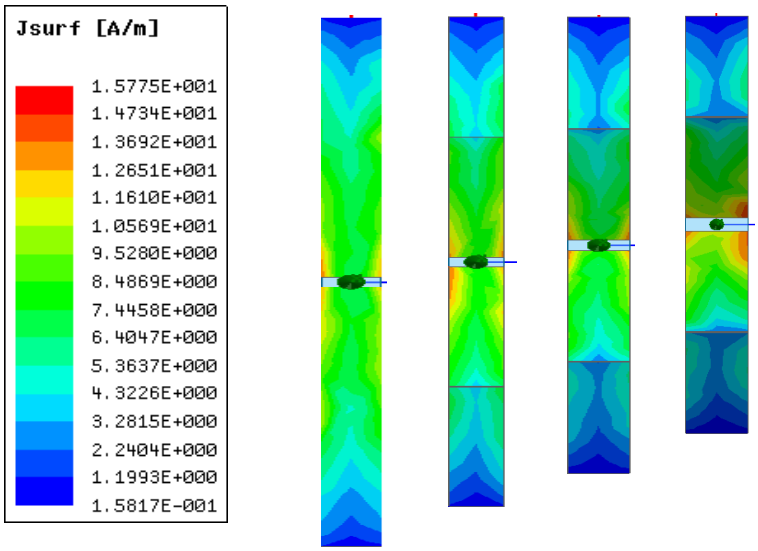

Figure 4.1: Simulated surface current upon the accordion-based dipole at: (a) φ = 0° (flat), (b) φ = 20°, (c) φ = 40°, and (d) φ = 60°.

The 10 dB bandwidths of the simulated antennas are identified from the corresponding $|S_{11}|$ plots, provided in Sections 4.2 and 4.3. The maximum bandwidth for the simulated ~160 mm copper antenna is observed at the 20° fold, while the maximum bandwidth for ~165 mm copper antenna occurs at 40°. The simulated ~160 mm antenna retains about 85% of the original 10-dB bandwidth, while the ~165 mm antenna retains about 93% of the original 10-dB bandwidth. The complete listing of the 10-dB bandwidths for the simulated antennas at all fold positions is given in Table 4.2.

Table 4.2: Simulated 10-dB bandwidths.

Position	Antenna Length: ~ 160 mm	Antenna Length: ~ 165 mm
0˚	0.129 GHz	0.108 GHz
20˚	0.140 GHz	0.108 GHz
40˚	0.110 GHz	0.122 GHz
60˚	0.110 GHz	0.100 GHz

Antennas of both dimensions exhibit similar, three-dimensional, toroidal radiation patterns. The E-plane and H-plane radiation patterns for the simulated ~165 mm copper antenna are provided in Section 4.3. Similar gain patterns are observed for the ~165 mm antenna at all fold angles in the simulation. A plot of the gain at the 40˚ position for the ~165 mm antenna, normalized to 0 dB, is provided in Section 4.3. At 40˚, the simulated maximum normalized gain is -0.77 dB.

4.2 Measurement Results Using RF Choke

The measured antenna reflection coefficient as a function of the angle φ is shown in Figure 4.2 for the ~160 mm antenna measured using the RF choke. In congruence with the simulated results, the resonance frequency increases as the antenna keeps folding. In fact, the antenna resonance frequencies are measured as 627 MHz, 760 MHz, 841 MHz, and 991 MHz for φ = 0° (flat), 20°, 40°, and 60°, respectively. The 10-dB antenna bandwidths are measured as 118 MHz, 133 MHz, 106 MHz, and 85 MHz for φ = 0° (flat), 20°, 40°, and 60°, respectively. These results indicate that the reconfiguration of the proof-of-concept E-textile origami dipole antenna enables more than a 55% change in resonance frequencies while retaining over 72% of the original 10-dB bandwidth.

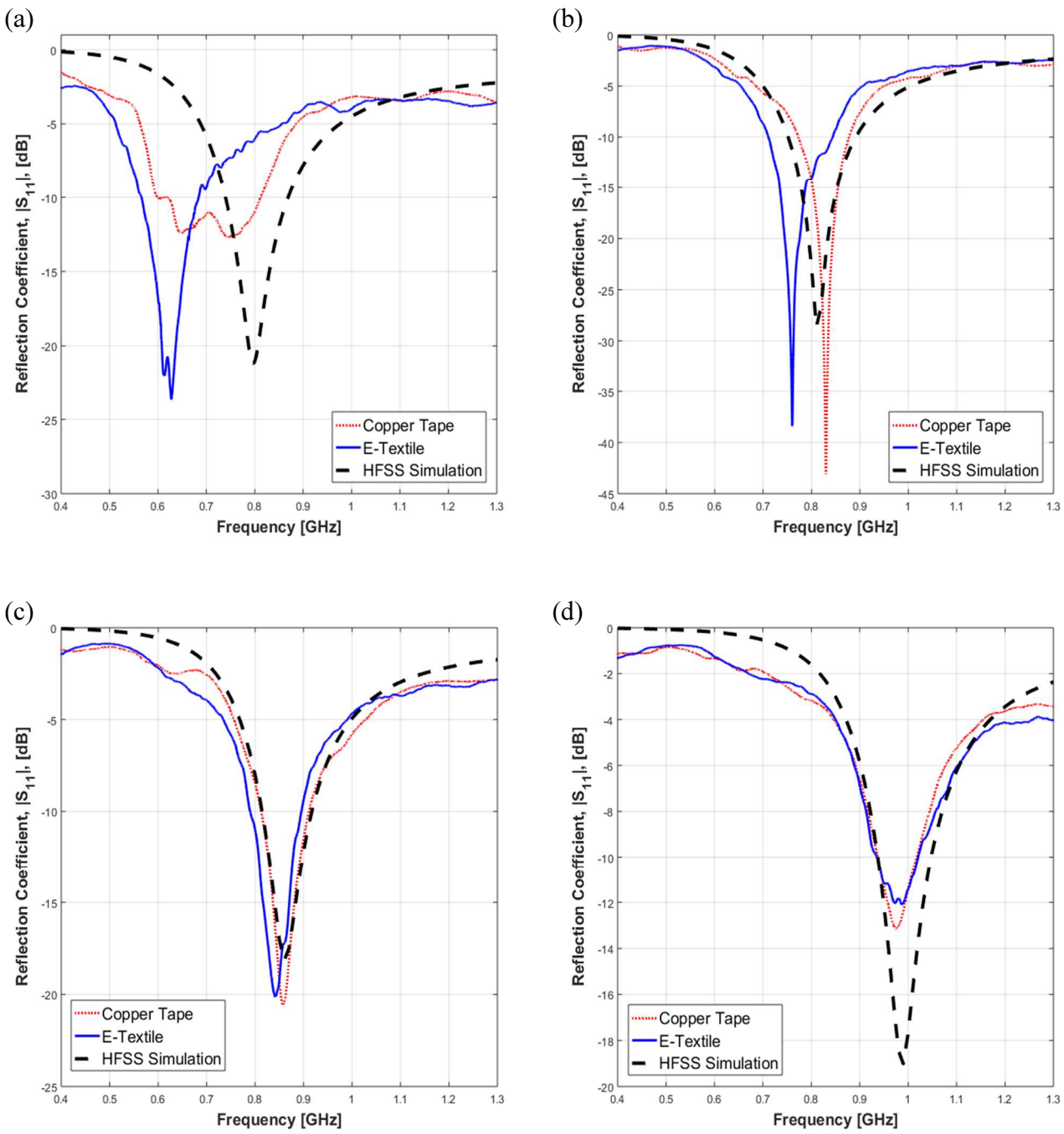

Figure 4.2: S11 results for ~160 mm antenna measured with RF choke at: (a) φ = 0° (flat), (b) φ = 20°, (c) φ = 40°, and (d) φ = 60°.

A complete listing of resonance frequencies and corresponding 10-dB bandwidths for the ~160 mm E-textile and copper antennas measured using the RF choke are shown in Tables 4.3 and 4.4, respectively. In both tables, the percent difference between E-textile and copper tape measurements is presented in the second to last column. Similarly, the percent difference between E-textile and simulation results is given in the final table column. Equation 7 provides the formula used to calculate the percent difference between two values (V_1 and V_2).

$$Percent\ Difference\ (\%) = \frac{|V_1 - V_2|}{\left(\frac{V_1 + V_2}{2}\right)} \quad (7)$$

For the 20°, 40°, and 60° positions, good agreement is observed between the E-textile measurements and simulation resonance frequencies, with a maximum percent difference of 6.369%.

Table 4.3: Resonance frequencies for ~ 160 mm antenna measured with RF choke.

Position	Resonance Freq. (GHz)		Percent Difference (%) between E-textile and:	
	Copper Tape	E-textile	Copper Tape	Simulation
0°	0.746	0.628	17.176	23.719
20°	0.830	0.760	8.805	6.369
40°	0.858	0.841	2.001	2.234
60°	0.975	0.988	1.325	0.202

Table 4.4: 10-dB bandwidths for ~ 160 mm antenna measured with RF choke.

Position	10-dB bandwidth (GHz)		Percent Difference (%) between E-textile and:	
	Copper Tape	E-textile	Copper Tape	Simulation
0°	0.203	0.118	52.960	8.907
20°	0.105	0.133	23.529	5.128
40°	0.099	0.106	6.829	3.704
60°	0.080	0.085	6.061	25.641

A significant difference between resonance frequencies for simulation and measurement is observed in the flat case, suggesting either inadequate current restriction by the employed RF choke, or electrical losses due to the proximity of the lab bench to the antenna. Both of these reasonings are accounted for in the ~165 mm measurements, in which: a) a bazooka balun tuned to the antenna's resonance frequency range is employed during measurements, and b) Styrofoam is used to provide additional separation between the antenna under test and the lab bench. While a balun was used to account for inadequate current restriction by the RF choke, alternative RF choke versions could have also been used. Specifically, in order to ensure balanced operation of the antenna, an RF choke of the correct size and material could be selected to provide current restriction at the resonance frequency of the antenna.

4.3. Measurement Results Using Bazooka Balun

The measured antenna reflection coefficient as a function of the angle φ is shown in Figure 4.3, for the ~165 mm antenna measured using the bazooka balun. As in the simulation and ~160 mm antenna cases, increased fold angles correspond to an increase in the resonance frequency due to a reduction in the projected antenna length. Specifically,

the antenna resonance frequency changes as 756 MHz, 783 MHz, 853 MHz, and 1014 MHz for φ = 0° (flat), 20°, 40°, and 60°, respectively.

Good agreement is achieved between the measured data and simulations, with a percent difference of <1.5% in the achieved resonance frequencies. The 10-dB bandwidth is measured as 80, 78, 89, and 77 MHz for φ = 0° (flat), 20°, 40°, and 60°, respectively, with a percent difference of <10% among all measurements. These results demonstrate a wide range of change in resonance frequency while maintaining around 96% of the initial 10-dB bandwidth.

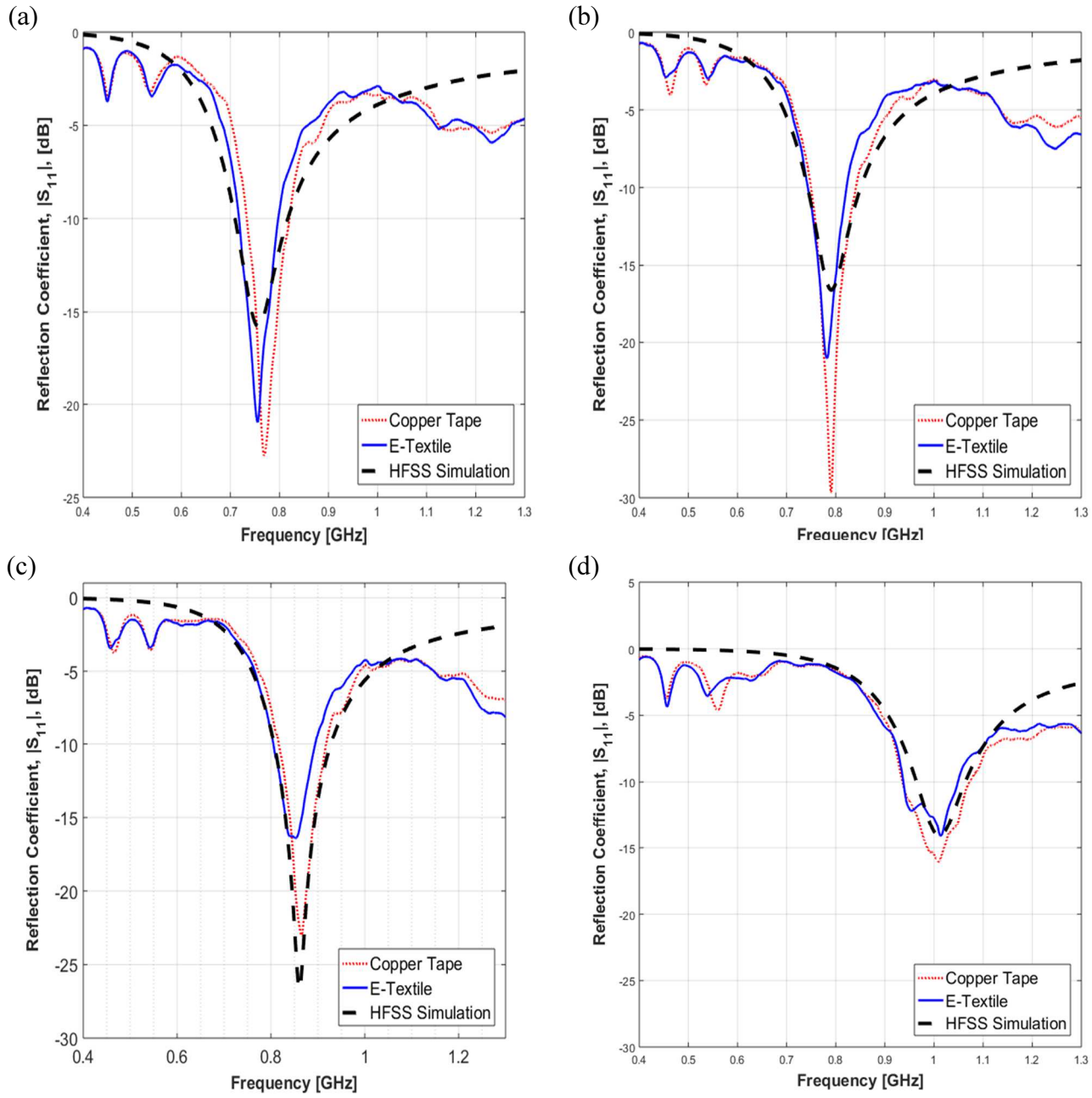

Figure 4.3: |S11| results for ~165 mm antenna measured with balun at: (a) φ = 0° (flat), (b) φ = 20°, (c) φ = 40°, and (d) φ = 60°.

As mentioned in Chapter 3.3, three bazooka baluns were used to measure the ~165 mm E-textile antenna. The operational regions for the bazooka baluns were approximately 650 to 800 MHz, 750 to 900 MHz, and 900 to 1150 MHz. At 0° the bazooka balun with an

operation region of 650 to 800 MHz was used, since the resonance frequency of the ~165 mm antenna fell within this range. Similarly, the 750 to 900 MHz balun was employed at the 20°, and 40° positions while the 900 to 1150 MHz balun was used at the 60° positions. Hence, the aforementioned plots can only be deemed valid within the respective operation regions of the baluns used at each fold position. The accuracy of the reflection coefficient values for frequencies that fall outside of the operational ranges of the respective baluns cannot be guaranteed.

A complete list of the resonance frequencies and corresponding 10-dB bandwidths for the ~165 mm E-textile and copper antennas measured using the bazooka balun are shown in Tables 4.5 and 4.6 respectively. As in Tables 4.3 and 4.4, the percent difference between E-textile and copper tape measurements as well as the percent difference between E-textile and simulation results are provided in the final two columns of both tables.

Table 4.5: Resonance frequencies for ~ 165 mm antenna measured with balun.

Position	Resonance Freq. (GHz)		Percent Difference (%) between E-Textile and:	
	Copper Tape	E-textile	Copper Tape	Simulation
0°	0.770	0.756	1.835	0.000
20°	0.790	0.783	0.890	1.143
40°	0.865	0.853	1.397	0.817
60°	1.016	1.014	0.197	0.197

Table 4.6: 10-dB bandwidths for ~ 165 mm antenna measured with balun.

Position	10-dB Bandwidth (GHz)		Percent Difference (%) between E-Textile and:	
	Copper Tape	E-textile	Copper Tape	Simulation
0°	0.088	0.080	9.524	29.787
20°	0.091	0.078	15.385	32.258
40°	0.101	0.089	12.632	31.280
60°	0.124	0.077	46.766	25.989

The E- and H-plane radiation patterns for all antenna fold positions are shown in Fig. 4.4 and further compared vs. the corresponding simulation results. Again, excellent agreement is observed between the simulations and measurements. Discrepancies are smaller than 0.2, 0.4, 0.5, and 0.7 dB for φ = 0°, 20°, 40°, and 60°, respectively. Increasing measurement errors with folding angles are associated with difficulties in feeding the antenna since the feed point coincides with a valley in the Styrofoam fixture, Figure 3.4 (b).

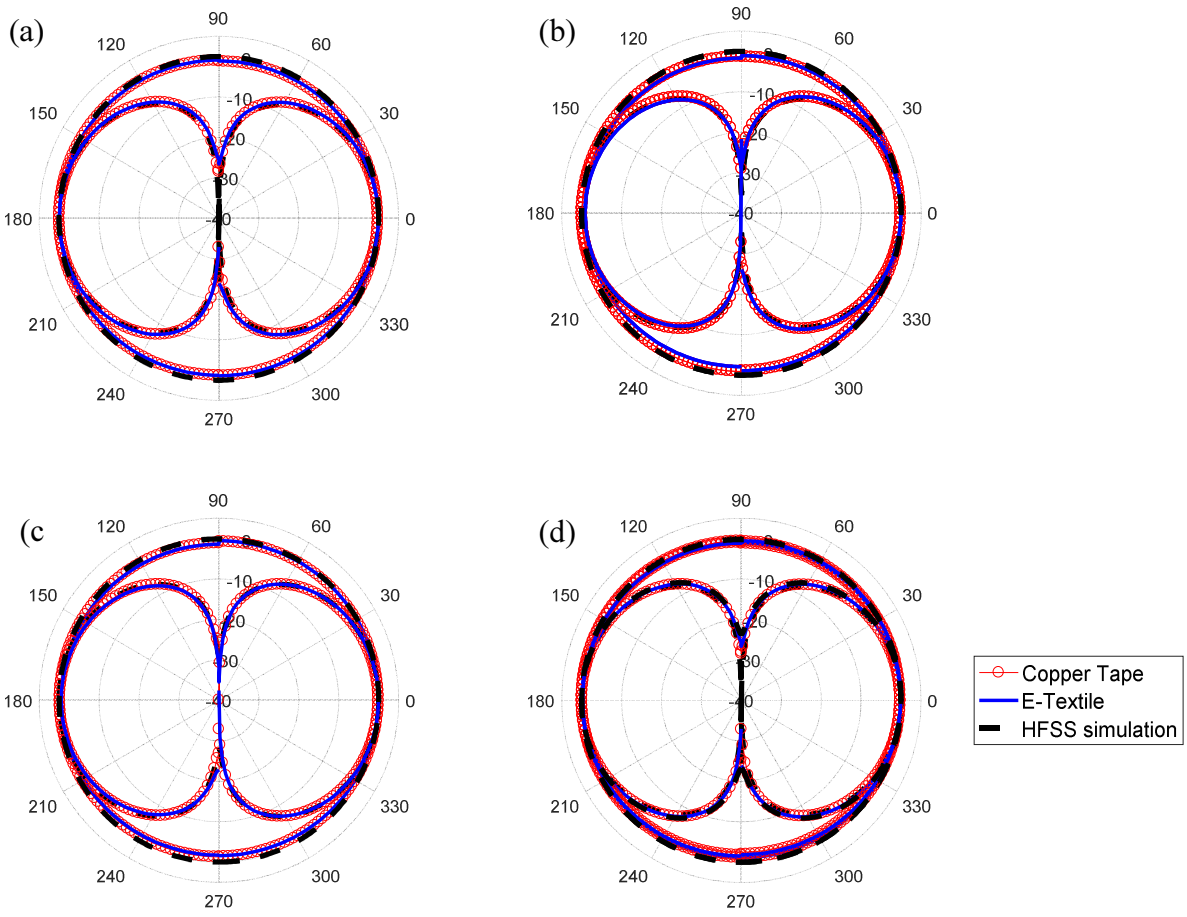

Figure 4.4: E-plane and H-plane radiation patterns for ~165 mm antenna measured with balun at: (a) φ = 0° (flat), (b) φ = 20°, (c) φ = 40°, and (d) φ = 60°.

The normalized maximum realized gain as a function of frequency for the example case of φ = 40° is shown in Fig. 4.5. The difference between measurements and simulations is within ~1 dB error, which lies within the measurement error range of the RFxpert. Furthermore, as expected, the maximum measured gain occurs near the resonance frequency.

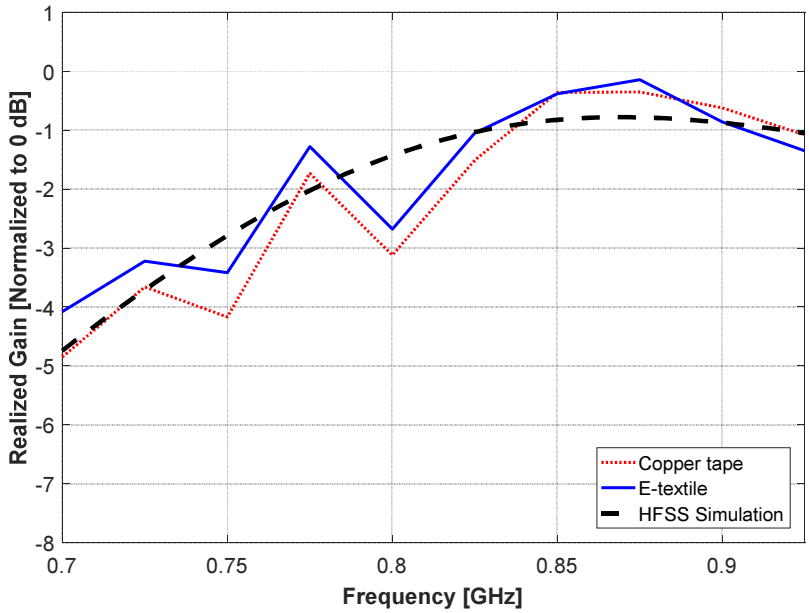

Figure 4.5: Normalized gain for ~165 mm antenna measured using balun at φ = 40°.

Chapter 5. Future Research Thrusts and Applications

5.1. Graded Embroidery Process for Enhanced Flexibility

The previous sections have described a novel, E-textile origami-based antenna that exhibits both impressive flexibility and mechanical durability. The proposed antenna consists of a uniform thread density in both conducting segments and hence exhibits constant flexibility at each point along the antenna. While this feature may be useful for certain applications in which the origami folding pattern is not predefined, the flexibility of the antennas can be optimized for a specified origami shape by reducing the thread density at the crease points. Such an E-textile antenna, as shown in Figure 5.1, would require a graded embroidery process in which a reduced thread density is first used to form the base of the antenna [36]. Afterwards, a higher thread density can be used to define the creases.

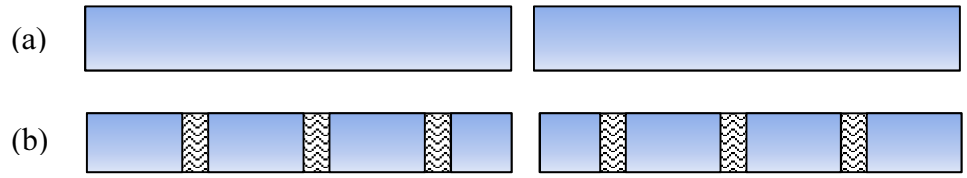

Figure 5.1: E-textile antenna with (a) uniform thread density and (b) reduced thread density at folds to enhance flexibility.

While employing a graded embroidery process will certainly result in improved antenna flexibility, the surface conductivity at the crease points is likely to decrease. Hence, further study is required to characterize the effects of reduced thread densities at the crease points on the antenna's operational parameters to ensure that the antenna's performance is not sacrificed.

5.2. Alternative Antennas

A half-wavelength dipole antenna was explored in this investigation due to wide practical use. However, the E-textile antenna fabrication process and origami operating principles detailed in this study can be easily applied to a wide variety of antenna types and origami folding patterns. Two specific antennas are described below.

Monopole Antenna: In principle, an origami-based monopole antenna would exhibit similar operational parameters as the half-wavelength dipole antenna. A monopole antenna consists of a conducting segment, supported below by a ground plane [28], Figure 5.2.

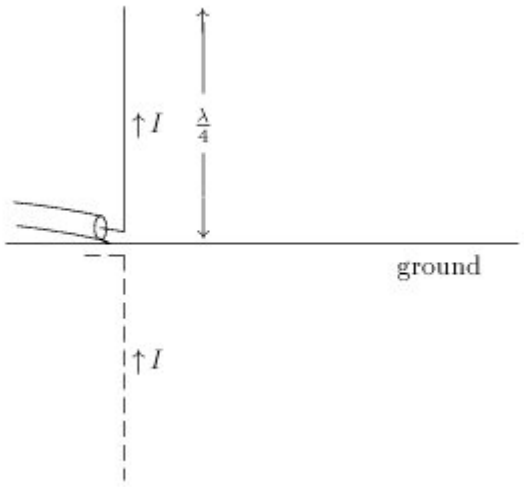

Figure 5.2: Quarter-wavelength monopole antenna [37]

As the length of the conducting segment of the monopole antenna increases, a corresponding decrease in the resonance frequency is expected. However, in contrast to the dipole antenna, the presence of a ground plane can allow the radiation pattern of the monopole antenna to be reconfigured as well. As the size of the conductive segment of the monopole antenna is reduced relative to the ground plane, the antenna will exhibit peak

radiation in the plane orthogonal to the monopole axis. Meanwhile, increasing the size of the conducting segment relative to the ground plane will cause the antenna to exhibit peak radiation at an angle above the plane orthogonal to the monopole axis. Therefore, a monopole antenna capable of reconfiguring the size of its conducting segment is capable of tuning both its resonance frequency and radiation pattern.

Patch Antenna: Patch antennas, also known as microstrip antennas, are becoming increasingly widespread in practice as they are low cost and can be directly printed onto circuit boards [28]. Patch antennas are powered by means of a microstrip transmission line. The patch antenna along with the microstrip transmission are placed above a dielectric substrate, which subsequently rests upon a ground plane as shown in Figure 5.3.

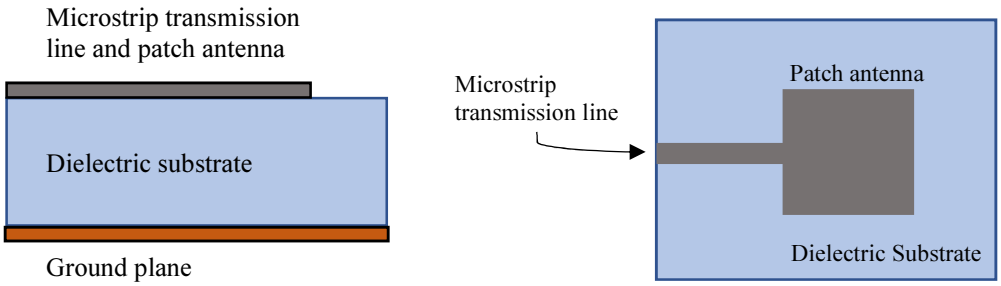

Figure 5.3: Patch antenna setup (a) side view and (b) top view [28].

The transmission line, antenna, and ground plane are typically composed of copper, or another metal that exhibits high conductivity [28]. The patch antenna can effectively be modeled as an open circuit transmission line [28]. At the center of the antenna, the current distribution is at a maximum while the voltage level is at zero. The voltage reaches a maximum level at the end of the patch antenna, and a minimum level at the feed point. The

fringing electric fields, present at the edges of the patch antenna, add in phase, causing the antenna to radiate [28]. The radiation caused by the movement of charge along the patch antenna and microstrip transmission line is cancelled by the presence of the ground place, which exhibits an equal and opposite current [28]. The resonance frequency (f) of the antenna is determined by the patch length (L) and the permittivity of the dielectric substrate (p), as shown in Equation 8 [28].

$$f \approx \frac{c}{2L\sqrt{p}} \quad (8)$$

Thus, a decrease in the patch length corresponds to an increase in the resonance frequency, as in the case of the half-wavelength dipole antenna. However, a decrease in the patch size caused by folding the antenna itself may cause the horizontal components of the fringing fields to become misaligned, thereby decreasing the gain and directivity of the antenna. Patch antennas can be designed to conform to a wide variety of fold configurations. Hence, further investigation is required to characterize the effects of different origami tessellation shapes on the performance of a patch antenna. To this end, the Laboratory of Sound and Vibration Research at The Ohio State University is currently researching the operational parameters of modular Miura-ori and accordion based patch antennas [38].

5.3. Applications

Smart-Clothes & Wireless Communications: One of the prominent protentional applications of the proposed origami-based antennas is for wearable devices. Because these antennas are composed of lightweight, durable E-threads, they can easily be integrated into clothing. The proposed E-textile antennas can also be implemented in passive radar systems and other wireless communication applications. For example, such antennas can be stitched into the uniforms or body gear of combat soldiers thereby providing a wide band of frequencies for communication without the need of additional bulky devices [39]. The frequency band of the antenna can be tuned either by the soldier's movements, or by physical mechanisms that are made part of the uniform. Such E-textile antennas can also be powered using sunlight, or conductive fluids [40]. These antennas can be integrated into commercial wearables products as well, to monitor human gestures and perhaps allow for hands-free operation of other electronic devices.

Space: Deploying antennas into space for global positioning system (GPS), military, or weather surveillance purposes are expensive tasks for companies. As a result, there is high demand for space-deployable antennas capable of actively adapting their performance to suit multiple applications [41]. The proposed origami-based, E-textile antenna is capable of achieving this type of performance. When mechanically reconfigured, the operating frequency range of the proposed antenna can be shifted according to the desired application. A user from Earth can control the antenna position in real-time by means of a software application [41]. Furthermore, in contrast to large, rigid antennas, reconfigurable, origami-based antennas can be conveniently deployed via limited size space shuttles.

Figure 5.4 demonstrates the stowed and deployed positions of a reconfigurable, helical antenna.

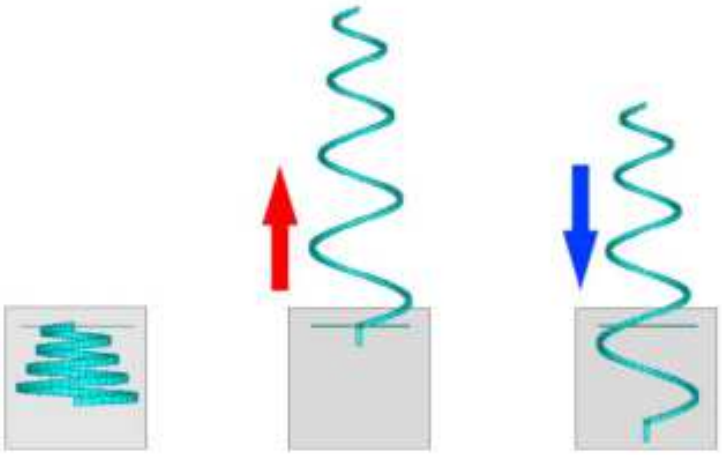

Figure 5.4: Stowed and deployed positions of a reconfigurable, helical antenna capable of being conveniently transported in a container of limited volume [41].

Medical Field: Radar-based microwave imaging by means of flexible, E-textile antennas can be used for early detection of breast and thyroid cancers. Microwave imaging systems require RF sensors capable of transmitting microwave signals to the object under test. These systems measure the electromagnetic radiation reflected by the object, and utilize computer software to visualize the electrical properties of the object being studied [42]. Microwave imaging systems have been successful in detecting cancerous tissues in patients [42-43]. These systems operate on the principle that cancerous cells contain a higher water and sodium concentrations compared to normal cells, and therefore exhibit different dielectric properties. By placing antennas or antenna arrays near the appropriate region of the body, the change of the antenna's performance due to the presence of water in the vicinity can be measured, and used to assist in the diagnosis of cancer [42-43]. However,

one of the major limitations of these systems is selecting the frequency of operation for which the antennas should be designed [42]. For this reason, researchers are currently investigating new “high dynamic measurement” systems that are both “compact and low-cost” [42]. The proposed E-textile antennas exhibit such dynamic behavior, and can be reconfigured to operate at the frequency range required to detect malignant tissues via microwave imaging. Furthermore, by transmitting a wide range of microwave frequencies to the tissue under test, a more accurate image of the tissue may be obtained. These antennas are lightweight and inexpensive, and hence can be easily stitched into the clothing of patients for continuous tissue monitoring. Furthermore, the proposed E-textile antennas can easily conform to the chest and neck regions of the body, and therefore can provide additional comfort to the patient without sacrificing performance.

Chapter 6. Conclusion

Origami antennas reported to date typically employ copper tapes and conductive inks to realize the conductive segments, and paper to realize the antenna substrate. As a result, these antennas exhibit a limited lifetime due to the inherent fragility of their underlying materials. In contrast, the origami antennas proposed in this research rely on mechanically robust yet flexible E-threads. Feasibility of the proposed approach was demonstrated using two accordion-based, half-wavelength dipole antennas with dimensions ~160 mm × 10 mm and ~165 mm × ~10 mm. As the ~160 mm antenna was folded, the resonance frequency was tuned from 627 MHz to 991 MHz while retaining 77% of the original 10-dB bandwidth. By folding the ~165 mm dipole, the resonant frequency was shifted from 756 to 1014 MHz while retaining 96% of the original 10-dB bandwidth.

The diverse applications of these antennas include wearable sensors, wireless communications, space electronics, and medical devices. Future work will focus on optimizing the flexibility of the antennas for specific folding patterns, and exploring the operational properties of alternative origami-based antenna configurations.

References

[1] N. Haider, D. Caratelli, A. G. Yarovoy, "Recent developments in reconfigurable and multiband antenna technology," in *International Journal of Antennas and Propagation*, 2013, pp. 1–14, 2013.

[2] R. L. Haupt, M. Lanagan, "Reconfigurable antennas," in *IEEE Antennas and Propagation Magazine*, vol. 55, no. 1, pp. 49-61, Feb. 2013.

[3] J. Costantine, Y. Tawk, S. E. Barbin, C. G. Christodoulou, "Reconfigurable antennas: Design and applications," in *Proc. IEEE*, vol. 103, no. 3, pp. 424-437, Mar. 2015.

[4] S.M. Saeed, C.A. Balanis, C.R. Birtcher, A.C. Durgun, and H.N.Shaman, "Wearable flexible reconfigurable antenna integrated with artificial magnetic conductor," in *IEEE Antennas and Wireless Propagation Letters*, vol. 16, pp. 2396-2399, Jun. 2017.

[5] S. Yan and G.A.E. Vandenbosch, "Radiation pattern-reconfigurable wearable antenna based on metamaterial structure," in *IEEE Antennas and Wireless Propagation Letters*, vol. 16, pp. 1715-1718, Feb. 2016.

[6] H. Giddens, L. Yang, J. Tian, and Y. Hao, "Mid-infrared reflect-array antenna with beam switching enabled by continuous graphene layer," in *IEEE Photonics Technology Letters*, vol. 30, no. 8, pp. 748-751, Apr. 2018.

[7] H. Wang, Y. Wang, et al., "Small-size reconfigurable loop antenna for mobile phone applications," in *IEEE Access*, vol. 4, pp. 5179-5186, Jul. 2016.

[8] X. Liu, S. Yao, B. S. Cook, M. M. Tentzeris and S. V. Georgakopoulos, "An origami Reconfigurable Axial-Mode Bifilar Helical Antenna," *IEEE Transactions on Antennas and Propagation*, vol. 63, no. 12, pp. 5897-5903, Dec. 2015.

[9] S. J. Mazlouman, A. Mahanfar, C. Menon, and R. G. Vaughan, "Reconfigurable axial-mode helix antennas using shape memory alloys," in *IEEE Transactions on Antennas and Propagation*, vol. 59, no. 4, pp. 1070–1077, Apr. 2011.

[10] S.I.H Shah, D. Lee, M. Tentzeris, and S. Lim, "A Novel High-Gain Tetrahedron origami," in *IEEE Antennas and Wireless Propagation Letters*, vol. 16, pp. 848-851, Sept. 2016.

[11] X. Liu, S.V. Georgakopoulos, and S. Rao, "A Design of an origami Reconfigurable QHA with a Foldable Reflector," in *IEEE Antennas and Propagation Magazine*, vol. 59, no. 4, pp. 78-105, Aug. 2017.

[12] G. J. Hayes, Y. Liu, J. Genzer, G. Lazzi, and M. D. Dickey, “Self- Folding origami Microstrip Antennas,” in *IEEE Transactions on Antennas and Propagation*, vol. 62, no. 10, pp. 5416-5419, Oct. 2014.

[13] S. Yao, X. Liu, J. Gibson, S. V. Georgakopoulos, “Deployable origami Yagi loop antenna,” in *Proc. IEEE Antennas and Propagation Society International Symposium*, pp. 2215-2216, Jul. 2015.

[14] J. Kimionis, M. Isakov, B. S. Koh, A. Georgiadis, and M. M. Tentzeris, “3D-printed origami packaging with inkjet-printed antennas for RF harvesting sensors,” in *IEEE Transactions on Microwave Theory and Techniques.*, vol. 63, no. 12, pp. 4521–4532, Dec. 2015.

[15] S. I. Hussain Shah and S. Lim, "Frequency switchable origami magic cube antenna," in *2017 IEEE Asia Pacific Microwave Conference (APMC)*, Kuala Lumpar, pp. 105-107, 2017.

[16] S. Yao, X. Liu and S. V. Georgakopoulos, "Morphing Origami Conical Spiral Antenna Based on the Nojima Wrap," in *IEEE Transactions on Antennas and Propagation*, vol. 65, no. 5, pp. 2222-2232, May 2017.

[17] S. Jun, J. Heirons and B. Sanz-Izquierdo, "Inkjet printed dual band antenna for paper UAVs," in *2017 11th European Conference on Antennas and Propagation (EUCAP)*, Paris, pp. 3452-3456, 2017.

[18] S. Alharbi, R. Shubair, and A. Kiourti, “Flexible antennas for wearable applications: recent advances and design challenges,” in *Proc. European Conf. Antennas Propag. (EUCAP)*, London, UK, April 9-14, pp. 9-13, 2018.

[19] C. Zou, S. Chaudhari, S. Alharbi, H. Shah, A. Kiourti, and R.L. Harne, “Investigation of Reconfigurable Antennas by Foldable, E-textile Tessellations: Modeling and Experimentation,” in *Proc. 175th Meeting of the Acoustical Society of America*, Minneapolis, MN, May 7–11, p. 1955, 2018.

[20] S. Chaudhari, S. Alharbi, C. Zou, H. Shah, R.L. Harne, and A. Kiourti, “A New Class of Reconfigurable Origami Antennas Based on E-textile Embroidery,” in *2018 IEEE International Symposium on Antennas and Propagation*, Boston, MA, Jul. 08–13, p. 1196, 2018.

[21] A. Kiourti and J.L. Volakis, “Conductive Textiles for Wearable Electronics,” in *International Symposium on Electromagnetic Theory (EMTS 2016)*, Espoo, Finland, Aug. pp. 14–18, 2016.

[22] R.L. Harne and D.T. Lynd, “Origami acoustics: using principles of folding structural acoustics for simple and large focusing of sound energy,” in *Smart Materials and Structures*, vol. 25, p. 085031, 2016.

[23] D.T. Lynd and R.L. Harne, “Strategies to predict radiated sound fields from foldable, Miura-ori-based transducers for acoustic beamfolding,” in *The Journal of the Acoustical Society of America*, vol. 141, pp. 480-489, 2017.

[24] C. Zou and R.L. Harne, “Adaptive acoustic energy delivery to near and far fields using foldable,tessellated star transducers,” in *Smart Materials and Structures*, vol. 26, p. 055021, 2017.

[25] C. A. Balanis, Antenna Theory and Design, 3rd ed. Hoboken, NJ: John Wiley, 2005.

[26] S. Turner, "General Question of the Week G9B08 Dipole Impedance | Ham Radio School.com", *Ham Radio School.com*, 2018. [Online]. Available: https://hamradioschool.com/general-question-of-the-week-g9b08-dipole-impedance/. [Accessed: 14- Oct- 2018].

[27] En.wikipedia.org. (2018). *Dipole antenna*. [online] Available at: https://en.wikipedia.org/wiki/Dipole_antenna [Accessed 14 Oct. 2018].

[28] Bevelacqua, P. (2018). *The Antenna Theory Website*. [online] Antenna-theory.com. Available at: http://www.antenna-theory.com/ [Accessed 14 Oct. 2018].

[29] *Wikipedia*. [Online]. Available at: https://tk.m.wikipedia.org/wiki/Faýl:Electric_field_point_lines_equipotentials.svg . [Accessed: 14-Oct-2018].

[30] Ansys High Frequency Structure Simulator. Available: https://www.ansys.com/products/electronics/ansys-hfss

[31] M. Kopp, *An Introduction to HFSS: Fundamental Principles, Concepts, and Use*. Ansoft, LLC.

[32] “Introduction to finite element analysis,” *OpenLearn*. [Online]. Available: http://www.open.edu/openlearn/science-maths-technology/introduction-finite-element-analysis/content-section-1.7. [Accessed: 21-Oct-2018].

[33] COMSOL Multiphysics®. Available: https://www.comsol.com/

[34] Brother PE-DESIGN. Available: https://www.brotherusa.com/products/pedesign10

[35] A. Kiourti, C. Lee, and J.L. Volakis, “Fabrication of textile antennas and circuits with 0.1mm precision,” in *IEEE Antennas and Wireless Propagation Letters*, vol. 15, pp. 151–153, 2015.

[36] S. Alharbi *et al*., "E-textile Origami Dipole Antennas with Graded Embroidery for Adaptive RF Performance," in *IEEE Antennas and Wireless Propagation Letters*.

[37] *Wikipedia*. [Online]. Available at: https://commons.wikimedia.org/wiki/File:A6-3EN.jpg. [Accessed: 21-Oct-2018].

[38] H. Shah, A. Inshaar, C. Zou, S. Chaudhari, S. Alharbi, A. Kiourti, and R.L. Harne. "Multiphysics modeling and experimental validation of reconfigurable, E-textile origami antennas." in *Proc. ASME 2018 International Design Engineering Technical Conferences*, DETC2018-85603, Quebec City, Canada, p. V05BT07A057, Aug 2018.

[39] S. I. H. Shah, Sungjoon Lim and M. M. Tentzeris, "Military field deployable antenna using origami," in *2017 International Workshop on Antenna Technology: Small Antennas, Innovative Structures, and Applications (iWAT)*, pp. 72-73, Athens, 2017.

[40] R. Vilkhu, W. J. Thio, P. Das Ghatak, C. K. Sen, A. C. Co and A. Kiourti, "Power Generation for Wearable Electronics: Designing Electrochemical Storage on Fabrics," in *IEEE Access*, vol. 6, pp. 28945-28950, 2018.

[41] C. Christodoulou, "Multifunctional Reconfigurable/Deployable Antennas for Space Applications," in *Aiaa Space 2016*, Sep. 2016.

[42] L. Wang, "Microwave Sensors for Breast Cancer Detection," in *Sensors*, vol. 18, no. 65, p. 655, 2018.

[43] R. S. I and J. T, "Design and implementation of flexible wearable antenna on thyroid gland in the detection of cancer cells," in *Biomedical Research*, vol. 29, no. 11, pp. 2307-2312, 2018.